

ISSN 1335-8871

MEASUREMENT SCIENCE REVIEW



Journal homepage: https://content.sciendo.com

Filter and Sampling Rate Optimization for PPG-Based Detection of Autonomic Dysfunction: An ECG-guided Approach

Yi-Hui Kao^{-1,2}, Danyal Shahmirzadi³, Sung-Tsang Hsieh^{4,5,6,7,8}, Wen-Fong Wang^{9*}

Abstract: Photoplethysmography (PPG) is well suited for wearable health applications, but has a lower frequency spectrum than electrocardiography (ECG) and is more affected by motion artifacts. In this study, ten signal filters from three categories were investigated in combination with different sampling rates to evaluate their effects on PPG signal quality. A correlation and accuracy analysis was performed comparing the interbeat intervals detected in PPG and ECG using Pearson correlation and absolute error. The results showed that specific filters with sampling rates as low as 40 Hz perform well in detecting autonomic neuropathy. The results highlight the potential of PPG with optimized filters and sampling rates for clinical screening of the autonomic nervous system (ANS) in wearable health monitoring.

Keywords: photoplethysmography, electrocardiography, healthcare, wearable, autonomous, neuropathy

1. Introduction

The autonomic nervous system (ANS) controls the nonstriated muscles and glands and can be divided into three sympathetic (thoracolumbar), parasympathetic (craniosacral), and enteric nervous system. The cardiac autonomic plexus is supplied by the cardiac nerves, which originate from the cervical and upper thoracic sympathetic ganglia (sympathetic) and the cardiac branches of the vagus nerves (parasympathetic). The most widely used examination for testing cardiac vagal tone is the variation of interbeat intervals, i.e. the variation of the R-R interval (RRIV) [1]. The RRIV can be reliably derived from electrocardiography (ECG) data, extracting the R peaks from one QRS complex to the next R peak intervals (RRIs) with millisecond accuracy. The RRI is not a fixed value, and the normal sinus arrhythmia is the heart rate (HR) variability that occurs with respiration. The phenomenon is significant in healthy people and occurs mainly in the young group. Sinus arrhythmia usually becomes less pronounced with increasing age and may be significantly impaired or abolished if the vagal innervation of the heart is impaired.

The HR response to deep breathing shows maximum variability at a breathing rate of about 5 to 6 per minute [2]. Therefore, RRIV can be derived both at rest and during deep breathing to assess the ANS. In most autonomic system dysfunctions, the HR tends to be consistent at rest and during deep breathing. The lack of normal variability results in an inability to adapt to changes and low RRIV values. In contrast, in some patients with autonomic dysfunction, RRI increases irregularity and results in a significantly elevated RRIV above the normal range. However, to investigate these phenomena, routine RRIV screening requires experienced technicians to attach ECG electrodes to the limbs and maintain full participation. This makes screening for autonomic system dysfunction a problem in daily life.

Photoplethysmography (PPG) is a simple, safe, common and convenient method of recording blood oxygen saturation

DOI: 10.2478/msr-2025-0024

*Corresponding author: wwf@yuntech.edu.tw (Wen-Fong Wang)

¹Department of Medical Education and Research, National Taiwan University Hospital Yun-Lin Branch, Douliu 640, Taiwan, blueggobi@gmail.com

²Graduate Institute of Anatomy and Cell Biology, National Taiwan University College of Medicine, Taipei, Taiwan ³Graduate School of Engineering Science and Technology, National Yunlin University of Science and Technology, 123 University Road, Douliou, 64002, Yunlin, Taiwan, d11010210@yuntech.edu.tw

⁴Department of Neurology, National Taiwan University Hospital, Taipei, Taiwan, shsieh@ntu.edu.tw

⁵Graduate Institute of Brain and Mind Sciences, National Taiwan University College of Medicine, Taipei, Taiwan

⁶Graduate Institute of Clinical Medicine, National Taiwan University College of Medicine, Taipei, Taiwan

⁷Center of Precision Medicine, National Taiwan University College of Medicine, Taipei, Taiwan

⁸Department of Anatomy and Cell Biology, National Taiwan University College of Medicine, Taipei, Taiwan

⁹Department of Computer Science and Information Engineering, National Yunlin University of Science and Technology, Douliu 640, Yunlin, Taiwan, wwf@yuntech.edu.tw

and arterial pulsation through the skin. It has also been attempted to detect different physiological characteristics and disease syndromes such as autonomic nervous function [3], respiratory rate estimation [4], metabolic syndromes [5], features of arteriovenous fistula stenosis in hemodialysis patients [6], etc. PPG sensors use light-based techniques to detect blood flow rates controlled by cardiac pumping action. The systolic peaks in the blood vessels correlate closely with the R waves in the ECG through a consistent delay, the pulse transit time [7]. By measuring the interval between one systolic peak and the next systolic peak of the PPG (SSI), we were able to infer the RRIV from the variation of SSIs (SSIV). In other words, we tried to simulate the electrical signals of the heart by arterial hemodynamic changes. Therefore, the calculation of RRIV requires highly accurate measurement of the maximum and minimum values of RRIs. It remains to be determined whether SSI is effective in calculating pulse rate variation, as few clinical studies have used SSIV to detect autonomic neuropathy.

To assess cardiac autonomic function, RRIV derived from the interbeat intervals of ECG is the most important feature accepted by neurologists. Due to the interference of lowfrequency noise caused by motion artifacts [8], the temporal positions of the reference points determined by different filters at different sampling rates can be significantly altered and affect the calculation of the interbeat variations, i.e. the RRIV or even the SSIV. The more accurately the reference points (such as the peaks of the PPG systole, the PPG first derivative, and the PPG second derivative waves [9]) on the PPG waveforms mark the interbeat intervals, the more effectively the variation can be determined by careful signal analysis [8]. Thus, it can be seen that there are two key factors, namely the filter and the available sampling rate, to obtain accurate PPG derived features. However, prior to our work, these two factors have not been further investigated or analyzed, especially at different sampling rates below 1000 Hz.

In this study, a number of filters belonging to the infinite impulse response (IIR), finite impulse response (FIR), and wavelet transform (WT) types were selected to process the PPG signals after signal pre-processing and to localize the most appropriate PPG systolic peaks in the cardiac cycles. The Butterworth [10], Bessel [11], Chebyshev [12] and Elliptic [13] filters were selected for the IIR filters, and the Savitzky-Golay [14], Average [15], and periodic moving average [16] filters were selected for the FIR filters. Since the WT includes the discrete wavelet transform (DWT) and the continuous wavelet transform (CWT), the selected WT filters with different mother wavelets such as Daubechies [17], Coiflet [18], and Morlet [19] were considered in the study. As a result, ten specific filters are used to verify whether wearable devices with PPG are a potential surrogate for autonomic dysfunction detection.

Due to the limited resources of wearable devices in terms of communication and computer hardware/software, sampling rates in signal acquisition can be much lower than similar procedures performed in laboratories or clinical examinations. For example, the PPG-powered sampling rate of wearable devices is reported as 200 Hz in [20], 100 Hz in [3], and 64 Hz in [21], which is much lower than the PPG

sampling rate of the PPG performed in our study. Recently, there is another viable PPG application in smartphones, the video-based PPG [22]. Its sampling rate is even downscaled to 25 Hz. In this study, we will simultaneously investigate the correlation and accuracy of the above filters under the influence of relatively low sampling rates.

In this article, Section 2 describes the methods for preparing the experimental and test environment, installing the test instruments, and signal processing to obtain the results of RRIV and SSIV. In Section 3, the results of PPG-based cardiac autonomic function screening are compared with the ECG results, and some discussions are made in Section 4. Finally, conclusions are drawn in Section 5.

2. LITERATURE REVIEW

While previous studies focused on removing motion artifacts from ECG or PPG signals individually, this study compares the effects of different filtering methods and sampling rates on PPG signals, using the ECG signal as a ground truth reference. In [23], the Mexican hat WT is used to decompose the largest difference in the green channel between consecutive frames. The authors also introduce a recursive baseline-wander removal algorithm with an adaptive window that effectively eliminates baseline drift. Using this method, a mean absolute error (MAE) of 3.58 was obtained for HR detection. In [24], three different sampling methods for the detection of PPG signals are investigated: aggressive duty cycling (ADC), compressive sampling, and event-driven sampling. Of these, ADC offers the best balance between accuracy and simplicity, although it consumes more power than the other two methods. The study found that 82 % of PPG sensors with a power consumption of less than 500 μW use ADC for sampling. Event-driven sampling, which minimizes power consumption by activating the LED only when the next peak in the signal is predicted, is particularly suitable for portable applications with limited power supply. In [25], a Hampel filter is used in conjunction with a fourth-order Butterworth bandpass filter to effectively remove noise from PPG signals. The study evaluates the performance of their filtering approach by comparing it with the results of eight recent studies. The method achieved an MAE of 2.41 for systolic blood pressure prediction and 1.31 for diastolic blood pressure prediction, demonstrating remarkable accuracy in blood pressure estimation while effectively suppressing noise. This comparison highlights the robustness and effectiveness of their proposed filtering technique in the context of advanced PPG signal processing. rPPG-Toolbox is provided by [26], which uses Butterworth bandpass filter along with OpenFace [27] in practice, which can analyze head motion in a real video. They have tested their method with different datasets that have different sampling rates. The result shows that the PURE dataset with the plane-orthogonal-to-skin (POS) method has the better performance with an MAE of 3.67. In [28], the authors introduced a multi-filter multi-channel (MFMC) method to process PPG signals. Using this approach, they achieved an MAE of 2.13 mmHg for diastolic blood pressure detection and 3.52 mmHg for systolic blood pressure detection. They applied Savgol, Chebyshev II, and bandpass filter to both the ECG and the PPG.

In [29], the authors investigated the effects of reducing the sample rate on pulse rate variability (PRV). In particular, they investigated how reducing the sampling rate from 1000 Hz to 50 Hz affected the accuracy and reliability of PRV measurements. The study focused on five different reference points, including line-medium and medium interpolate points, as these were crucial for analyzing the characteristics of the signal.

The results showed that among the five reference points studied, the line-medium and medium interpolate points were particularly effective. These points enabled a significant reduction in the sampling rate of the PPG signal recorded from both the finger and the forehead to 50 Hz. Remarkably, this reduction did not lead to significant changes in the PRV indices compared to those obtained at a higher sampling rate of 1000 Hz.

This indicates that under the conditions investigated, it is possible to use a lower sampling rate without compromising the quality of the PRV analysis. The ability to maintain the accuracy of PRV measurements with a reduced sampling rate could lead to more efficient data acquisition and processing in practical applications where lower sampling rates may be desirable due to hardware or data storage limitations.

In [30], the authors investigated the effects of sampling rate on heart rate variability (HRV) and PRV by simultaneously collecting PPG and ECG data from 54 participants. Their results showed that PRV and HRV have different characteristics. PRV offers certain advantages as it can capture ANS activity in everyday situations, whereas ECG typically requires a clinical setting. In addition, PRV parameters can be accurately assessed at lower sampling rates compared to ECG parameters. A sampling rate of 100 Hz is recommended for robust measurements, although a rate of 40 Hz can also provide satisfactory results.

3. Subject & methods

The experiment in this study was conducted at the National Taiwan University Hospital (NTUH), Yunlin Branch. A total of 251 patients were recruited for the experiment, with IRB approval (No. 20180613RINA) issued by the Ethics Review Board of NTUH. The age distribution of patients ranged from twenty to sixty-nine years. The exclusion criteria apply to patients presenting with the following symptoms:

- atrial fibrillation,
- cardiac arrhythmia,
- frequent premature ventricular contraction (PVC), occurring several times in one minute, and
- severe involuntary movements, including tremors, which would cause significant motion artifacts in the recorded signals.

After applying the exclusion criteria, there were three patients with atrial fibrillation, one with cardiac arrhythmia, two with frequent PVCs, and one with tremors. Finally, seven patients were excluded from the experiment, and the total number of patients included was 244, including 115 men and 129 women. The exclusion rate was 2.78 %.

The experiment was divided into two test phases: a resting phase and a deep breathing phase. During the experiment, all participants were asked to sit comfortably on a chair with their hands flat on the table. In the resting phase, participants were asked to sit on the chair, relax, and take normal breaths. In the deep breathing phase, participants were asked to take six deep breaths within one minute, alternating between 5 seconds inhalation and 5 seconds exhalation. To record each phase, the ECG and PPG signals (see Fig. 2) were recorded simultaneously and continuously over a period of four minutes. We used three electrodes to record the ECG signals based on standard Lead II. Two ECG electrodes are attached to the front of the left (positive) and right wrist (negative), and one is attached to the top of the left leg (earth), as shown in Fig. 1. A reflective photosensor is placed over the fingernail of the left index finger to capture PPG signals.

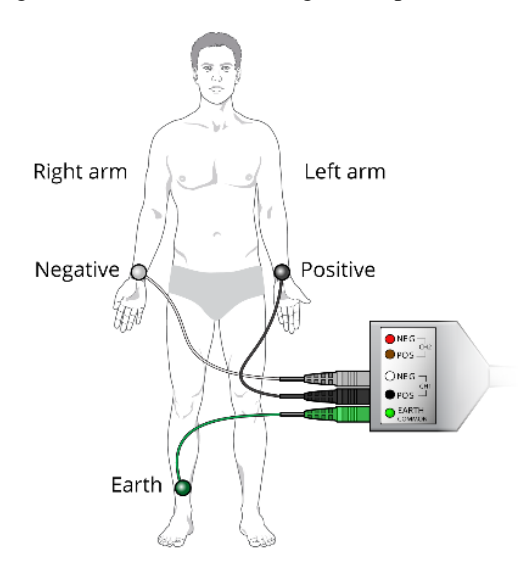


Fig. 1. The placement of the ECG electrodes with PowerLab, a physiological signal acquisition instruments from ADInstruments Inc. [30].

Test environment and instruments

In this study, Fig. 1 shows the environment and the instruments for signal acquisition. The physiological signal acquisition instruments, the PowerLab data acquisition device from ADInstruments [39], were used to acquire the ECG and PPG signals. This device is engineered for precise, consistent and reliable data acquisition and is connected to computers via USB links. With the support of the LabChart software package from ADInstruments [31], it can immediately display the acquired signals and store them as files for later analysis and reading. In this study, both signal sampling rates for ECG and PPG were set to 1000 Hz in the PowerLab system. It is worth noting that the resulting PPG signal with a 1000 Hz sampling rate is treated as the original signal to generate a downscaled PPG signal with a lower sampling rate. A lower sampling rate signal generation scheme is described below to obtain the lower sampling rates for the later experimental procedure in this study.

Down-sampling procedure for generating lower PPG sampling rates

To simulate lower sampling rates from the original PPG signal (sampled at 1 kHz), we applied a uniform downsampling method with a parameterized sampling period (per) defined in milliseconds.

Let:

PPGraw[n] be the raw PPG signal sampled at 1 kHz, where *n* is the signal length;

per be the sampling period in ms (e.g., $per = 10 \rightarrow 100 \text{ Hz}$); S[i] be the down-sampled PPG signal.

The pseudocode below describes the process:

This procedure was implemented in Python, using basic list indexing for down-sampling. The parameter per directly determines the sampling rate (e.g., per = 1 ms = 1000 Hz, per = 10 ms = 100 Hz, etc.).

In this study, the following sampling periods were used to generate lower-rate signals:

Sampling_periods = {2, 4, 5, 8, 10, 20, 25, 40, 50}, corresponding to frequencies between 20 Hz and 500 Hz. The lowest assumed sampling rate is 20 Hz for the application of video-based PPG [22].

Physiological signal processing

After the acquisition of ECG and PPG signals, the signal processing flow, shown in Fig. 3, consists of four stages, namely preprocessing, feature finding, signal decomposition and feature calculation, and performance measurement.

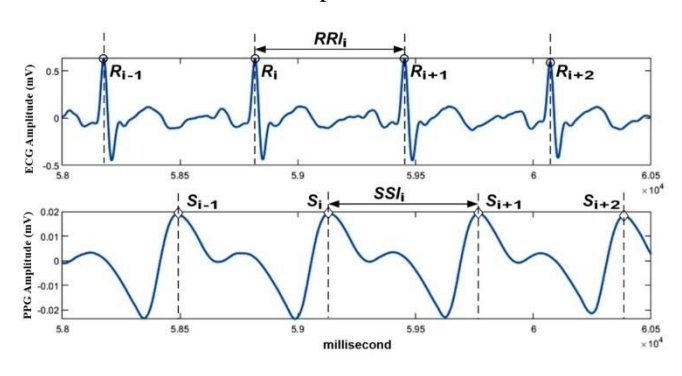


Fig. 2. Examples of ECG and PPG signals.

It should be noted that PPG signals are more susceptible to interference from baseline wander noise than ECG signals [8]. As in Stage 1 of Fig. 3, a baseline wander noise removal algorithm is developed to remove the baseline wander noise that was present in the raw ECG and PPG signals during preprocessing. To find the features of the signals after removing the baseline wander noise, the Pan-Tomkins algorithm was applied to localize the R peaks (marked as R_i in Fig. 2) in the cardiac cycles of the denoised ECG (Stage 2). At the same time, different filters were used to remove the PPG signals to localize the S peaks (marked as S_i in Fig. 2) in each cardiac cycle (Stage 2). Then, the two time domain features RRIi and SSIi (see Fig. 2) are calculated for ECG and PPG to determine the temporal length of each cardiac cycle

in Stage 3. Finally, performance measurements of the variation of interbeat intervals and the associated HRV parameters were performed. The acquired parameters are the RRIV and HRV of the ECG signal at 1000 Hz sampling rate, and the SSIV and associated HRV of the PPG signal at different down-sampling rates in Stage 4.

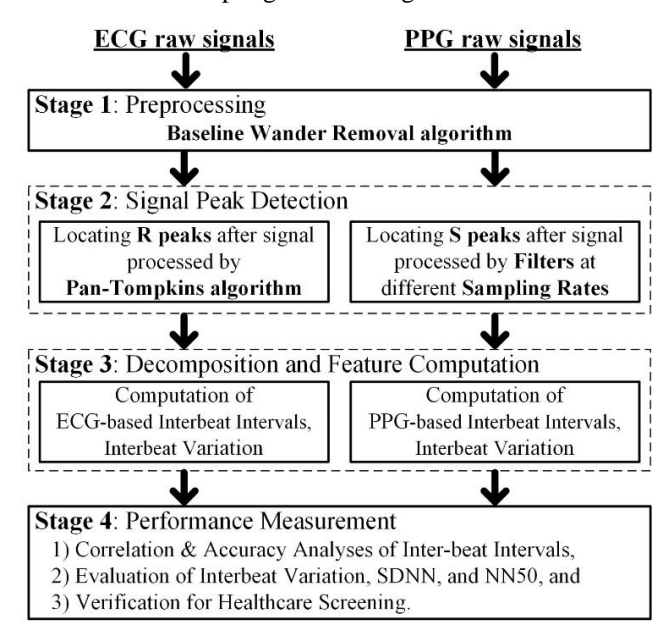


Fig. 3. Signal processing flow chart for ECG and PPG.

Stage 1: pre-processing

To remove the raw baseline wander in the ECG and PPG data, a baseline wander removal scheme based on the work of Chazal et al. [32] was considered. In two steps, the scheme uses a median filter [33] to filter out the core signals of ECG and PPG from the raw data. Chazal's method generates a baseline drift signal and uses it to offset the baseline wander with the raw data. In this way, a set of clear ECG or PPG signals is generated. The scheme is briefly described below.

Baseline wander removal by two-stage median filtering

To remove the baseline wander from the ECG and PPG signals, we applied a two-stage median filtering process as follows:

- **Step 1**: A median filter is applied to the raw signal using a shorter window size (*I*st_*WinSize*), resulting in the first filtered output.
- **Step 2**: A second median filter is then applied to the Step 1 output using a larger window size (2nd_WinSize).
- Step 3: The final baseline-corrected signal is obtained by subtracting the Step 2 output from the original raw signal.

Due to the different characteristics of ECG and PPG signals, different window sizes are used:

• For **ECG**:

 1^{st} _WinSize corresponds to 5 Hz (QRS wave) 2^{nd} _WinSize corresponds to 1.67 Hz (P and T waves)

• For **PPG**:

 I^{st} _WinSize corresponds to 1.6 Hz (systolic peak, similar frequency to P and T in ECG, in the experiment 1.6 Hz has the best performance)

2nd_WinSize corresponds to 0.5 Hz (diastolic peak)

This approach effectively suppresses the low-frequency drift while preserving the main features of the signal. These values were initially taken from the literature [40], [41] and then tested and fine-tuned to achieve the best results.

Stage 2: signal peak detection

For the detection of *R* peaks, a real-time QRS detection algorithm proposed by Pan and Tompkins is used to determine the temporal locations of all *R* peaks [34]. Since the Pan-Tompkins method is very efficient and powerful in detecting *R* peaks in baseline wander-free ECG signals, no further signal processing is required before detecting *R* peaks. Fig. 4 illustrates the process of extracting QRS from raw signals. After squaring the signal, all negative values were eliminated. Based on the above results for detecting the temporal location of each *R* peak, the interval of each pair of neighboring *R* peaks (i.e., RRI) can be determined, and thus, the RRIV variation (i.e., RRIV) can also be obtained.



Fig. 4. The process of extracting QRS from raw signals.

Since PPG signals are susceptible to motion artifacts, it is conceivable that PPG signals require careful signal processing to accurately detect PPG S peaks. In Table 1, four classical filters (Butterworth, Bessel, Chebyshev, and Elliptic), three smoothing filters (Savizky-Golay, average, and periodic moving average), and three wavelet-based filtering methods (Daubechies db6 (DWT), Coiflet C3 (DWT), and Morlet (CWT)) are tried to find the most

appropriate PPG S peak for each cardiac cycle. The classical filters (F01 to F04) have some outstanding features in signal filtering, but disadvantages in roll-off rate, pass/stopband ripple, and phase response [10]-[13]. Due to their low implementation complexity and low latency, they were used to determine the PPG S peak in this study. Then, the three smoothing filters (F11~F13) are considered since the PPG signal is not similar to the embedded ECG with the sharp QRS complex. These filters can provide different experimental aspects in detecting the PPG S peak. The wavelet-based methods (F21 to F23) include discrete and continuous wavelet transforms. For the DWT, Daubechies db6 and Coiflet C3 were used to perform a test for PPG signal processing, and Morlet was chosen for the CWT. Since these WT techniques have been used for ECG signal processing [35], it seems interesting to apply these methods to the PPG for investigation. The parameter settings required for the above filters are given in the description in Table 1.

To detect *S* peaks in the filtered PPG signal, a Python-coded peak search program was developed using a specific threshold value. Fig. 5 shows the results of the search for the ECG and PPG peaks.

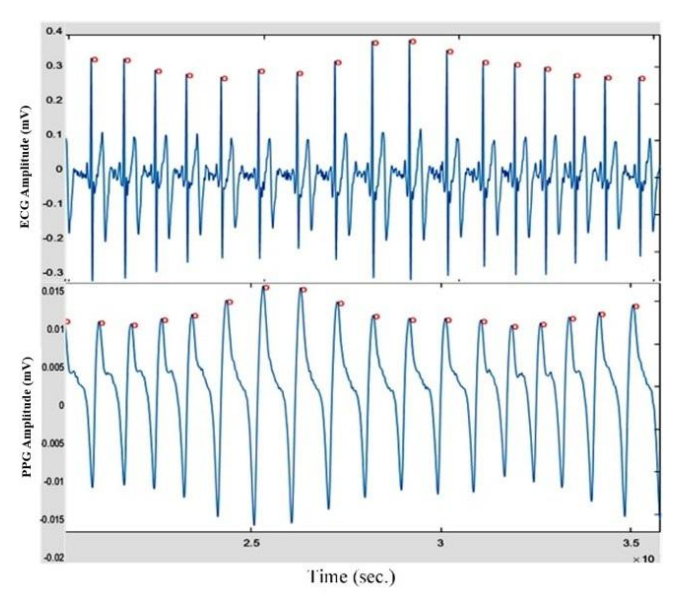


Fig. 5. Detected ECG and PPG peaks.

Tabl	e 1.	Α	descriptive	listing	ot	PPC	i signal	processing	g metho	ds.
------	------	---	-------------	---------	----	-----	----------	------------	---------	-----

No.	Filter name	Description
F01	Butterworth	The passband frequency is from 1 Hz to 5 Hz, and the filter order is 2.
F02	Bessel	
F03	Chebyshev	
F04	Elliptic	
F11	Savitzky-Golay	The polynomial order is 3, and the window size 401.
F12	Average	The passband frequency is from 1 Hz to 5 Hz.
F13	Periodic moving	After normalizing each cardiac cycle with the same number of sampled signals, the ith sampled signals of
		each of the 5 cycles are averaged, where $1 \le i \le$ the normalized cycle length.
F21	Daubechies	Use the inverse DWT of Daubechies db6 and Coiflet C3 to reconstruct the selected band from 1 Hz to 5 Hz.
F22	Coiflet C3	
F23	Morlet (CWT)	Apply the inverse WT of Morlet to reconstruct the selected band from 1 Hz to 5 Hz.

Stage 3: decomposition and feature calculation

After peak detection processing, as shown in Fig. 5, the continuous cardiac cycles in the ECG or PPG are decomposed and stored in an array $P(\bullet)$, which records a series of peaks. Then the interval between each pair of neighboring peaks, i.e., an RRI or SSI, can be calculated using (1).

$$Inter_Beat_Interval_i = P(i+1) - P(i)$$
 (1)

where $i \in \mathbb{Z}^+$, the set of positive integers.

Based on (1), let $IB_Interval$ be the set of all $Inter_Beat_Interval_i$, e.g., $\{Inter_Beat_Interval_i \mid i \in Z^+\}$. In this study, the method for calculating the interbeat variation in the ECG or PPG (i.e., the RRIV or SSIV) is shown in (2).

$$Variation = \frac{\max{(IB_Interval)} - \min{(IB_Interval)}}{\max{(IB_Interval)}} * 100\%$$
(2)

where the functions max (), min (), and mean () generate the maximum, minimum, and mean values for *IB Interval*.

Stage 4: performance measurement

To evaluate the effectiveness of SSI as an alternative to RRI, we used correlation and accuracy as performance metrics in this study. First, the correlation coefficients could be used to examine the trend of positive, negative, or no correlation between two discrete data sets. Let $\{r_1, r_2, \ldots, r_n\}$ and $\{s_1, s_2, \ldots, s_n\}$ be two data sets consisting of RRIs and SSIs, respectively. To measure the strength of a linear relationship between ECG and PPG parameters based on RRI and SSI, the Pearson correlation coefficient R_{rs} 3) is used. Through the correlation analysis, we can examine the closeness of the RRIs to the different SSIs obtained by the aforementioned preprocessing schemes (Table 1).

$$R_{rs} = \frac{n \sum r_i s_i - \sum r_i \sum s_i}{\sqrt{n \sum r_i^2 - (\sum r_i)^2} \sqrt{n \sum s_i^2 - (\sum s_i)^2}}$$
(3)

Second, we used the average absolute errors to evaluate the accuracy of the different SSIs from the PPG compared to the RRI from the ECG. After obtaining the RRI_i and SSI_i sets, i.e., $\{r_1, r_2, \ldots, r_n\}$ and $\{s_1, s_2, \ldots, s_n\}$, the average absolute error (Abs_{Err}) was calculated. For the performance evaluation of the interbeat variation, we evaluate the accuracy of the different SSIVs with respect to the RRIV using Abs_{Err} .

To investigate the applicability of the PPG-based solution for telemedicine and clinical applications, we include two HRV time domain parameters, SDNN and NN50, in addition to the interbeat interval and interbeat variation in the PPG in the accuracy evaluation [3]. In [36], the definition of SDNN is the standard deviation of all normal-to-normal intervals, and NN50 is the number of pairs of adjacent NN intervals that differ by more than 50 ms in the entire recording. In our study, the inclusion of SDNN and NN50 was essential for evaluating the validity of PPG-based detection of cardiac autonomic function.

Autonomic nervous system

To examine the use of PPG in screening for ANS disorders, the following four aspects of the examination are highlighted. The ANS regulates vital involuntary functions such as heart rate, blood pressure, and respiration through its sympathetic and parasympathetic branches. ANS dysfunction is associated with conditions such as diabetic neuropathy, cardiovascular disease, and postural orthostatic tachycardia syndrome (POTS). Due to its close connection to cardiovascular regulation, the ANS can be effectively monitored by non-invasive methods such as PPG:

- the assessment parameters used in ANS evaluation, such as interbeat interval (e.g., RRI, SSI), the interbeat variation (e.g., RRIV, SSIV), SDNN, and NN50;
- the filters used in PPG signal processing (see Table 1);
- the sampling rates used in PPG signal acquisition (e.g., 1000 Hz, 500 Hz, ..., 20 Hz);
- The effectiveness evaluation index includes the Pearson correlation and the average absolute error between the ECG and PPG parameters.

In this study, the RRI generated by the Pan-Tompkins algorithm is used as a criterion for comparison with the SSIs generated by the filters with different down-scaled sampling rates. To calculate a series of intervals in the ECG and PPG, (1) is applied to determine the RRI and different SSIs. Then, (2) is required to obtain the interbeat variation for the ECG and PPG series. Then, SDNN and NN50 were determined by RRI and the different SSIs to evaluate the validity of PPG-based detection of the cardiac autonomic function. To calculate the correlation coefficients, see (3) to evaluate the accuracy of using PPG as a substitute for ECG.

Since the physiological signals of the participants are recorded for four minutes in the resting phase and the deep breathing phase, each 4-minute signal unit is divided into the first and last 30-second signal units and three middle 1-minute signal units for analysis. For the sake of signal stability, the three units in the middle were used to calculate the evaluation parameters.

4. RESULTS

This section is divided into three subsections to provide a comprehensive overview of the main results obtained from the comparative analysis of different filtering methods and sampling rates applied to PPG signals.

A. Correlation and accuracy analysis of interbeat intervals in PPGs

To assess the validity of the interbeat interval in the PPG using the ECG evaluation criteria, Table 2 and Table 3 show the correlation coefficient and absolute error rate between the RRI at 1000 Hz and an SSI at different sampling rates.

Fig. 6 shows that the IIR filter bank performs better than the other filter banks in both the resting phase and the deep breathing phase. The four IIR filters are very similar in both phases, with the exception that Butterworth (F01) is slightly better than the other three. At the same time, each correlation coefficient (CC) value in the four IIR filters of the two phases

decreases linearly and slowly when the different sampling rates are examined. In Fig. 6, we can see that the IIR filter bank has very high CC values in both phases even at low sampling rates. This shows that the filter bank is suitable for wearables in healthcare.

For the other filters, F11 performs best in both phases at different sampling rates in the FIR filter bank, and its CC value is close to the CC values of the IIR filters. F23 outperforms the other two filters in the WT filter bank and its effectiveness is close to the IIR and F11 filters.

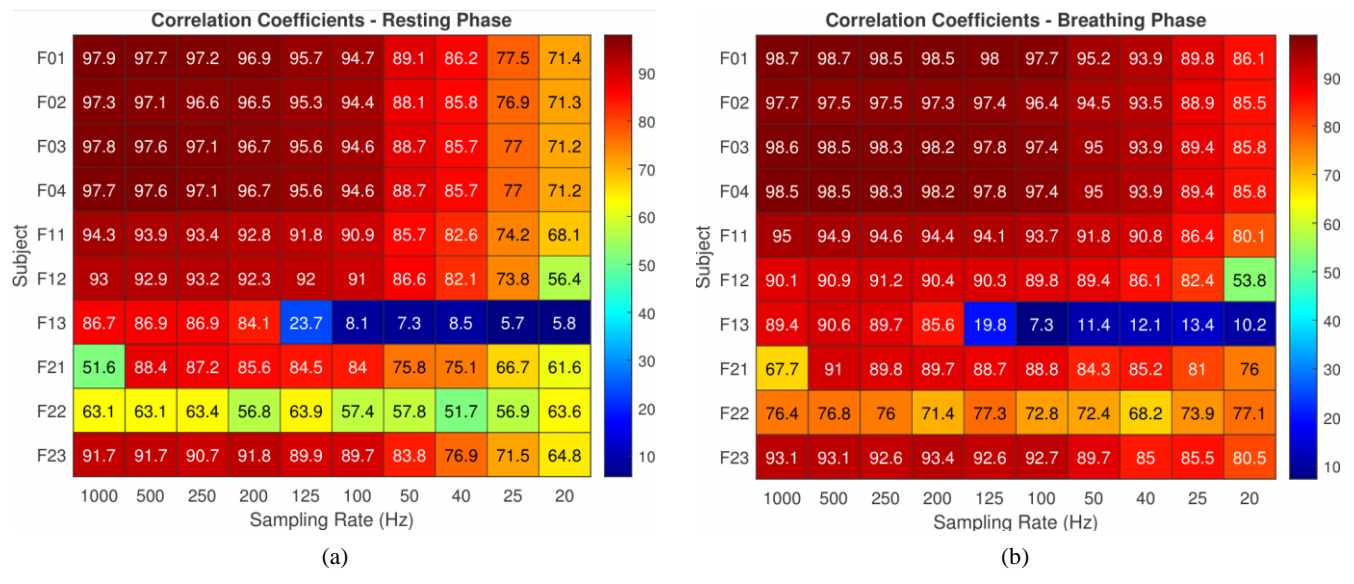


Fig. 6. HeatMap of correlation coefficients between the RRI at 1 kHz and the SSIs at various rates in resting (a), breathing phase (b).

 $Table\ 2.\ \ Average\ absolute\ errors\ between\ the\ RRIV/ECG\ SDNN/ECG,\ NN50\ at\ 1000\ Hz\ and\ the\ SSIV/PPG\ SDNN/PPG\ NN50\ at\ different\ sampling\ rates.$

Filter/	Phase	Parameter	1000	500	250	200	125	100	50	40	25	20
Sample rates			[Hz]									
F01	R	SSIV [%]	0.6	0.6	1.2	1.3	1.3	1.4	1.8	2.2	3.4	4.4
F11	R	SSIV [%]	1.4	1.5	2.1	2.2	2.3	2.3	2.8	3	4.1	7.3
F23	R	SSIV [%]	2	2.2	3	2.5	2.9	2.8	3.2	4.7	4.6	5.8
F01	В	SSIV [%]	0.9	1.1	1.2	1.1	1.2	1.2	1.8	2	2.9	3.8
F11	В	SSIV [%]	2.5	2.3	2.3	2.5	2.6	2.7	3.1	3.3	4.2	14.4
F23	В	SSIV [%]	2.6	2.7	2.9	2.5	2.9	3	3.4	5	4.3	5.6
F01	R	SDNN [ms]	0.6	0.6	0.6	0.6	0.8	0.9	2.1	3.1	6.5	9.5
F11	R	SDNN [ms]	1.3	1.4	1.5	1.6	1.7	1.9	3.2	4	7.3	12.4
F23	R	SDNN [ms]	2.7	2.6	2.8	2.1	2.7	2.3	3.4	6.9	7.5	10.8
F01	В	SDNN [ms]	1.2	1.2	1.3	1.3	1.3	1.4	2.2	2.7	5	7.2
F11	В	SDNN [ms]	2.2	2.2	2.2	2.4	2.4	2.6	3.3	3.9	6.3	15.3
F23	В	SDNN [ms]	2.7	2.7	2.9	2.4	2.7	2.6	3.3	6.1	5.6	8.1
F01	R	NN50 [%]	0.8	0.9	0.8	1	1	1.3	1.7	1.7	3.6	3.1
F11	R	NN50 [%]	1.7	1.6	1.8	1.6	1.9	2	3.5	2.2	5.1	4.3
F23	R	NN50 [%]	1.5	1.5	1.5	1.6	1.6	1.8	2.2	2.1	4.1	3.3
F01	В	NN50 [%]	0.8	0.8	0.8	0.9	0.9	1.1	2.2	1.8	3.6	3.1
F11	В	NN50 [%]	2.4	2.4	2.8	2.3	2.7	2.3	4.9	2.8	5.9	5.3
F23	В	NN50 [%]	1.6	1.6	1.7	1.6	1.7	1.9	3.1	2.5	4.8	4.1

Note: Phase R and B are resting and breathing phase, respectively.

Table 3. RRIV assessment range of normal cardiac autonomic function in each age group based on ECG [38].

Age [y]	20 ~ 29	30 ~ 39	40 ~ 49	50 ~ 59	60 ~ 69
Rest [ms]	12 ~ 46	6 ~ 32	6 ~ 36	5 ~ 23	7 ~ 19
Breath [ms] 19 ~ 62	9 ~ 54	14 ~ 48	11 ~ 59	8 ~ 28

Fig. 8 shows the absolute error, measured in microseconds, for all filters. For the IIR filter bank, it can be seen that the absolute errors of the filters are very low. Especially, at low sampling rates, the errors in both phases remain relatively low. This means that their accuracy is good enough for

wearable healthcare applications. For the FIR filter bank, F11 has the lowest absolute error, which is close to that of the IIF filter bank. For F12 and F13, the accuracy becomes very poor in both phases below 25 Hz and 200 Hz, respectively. Therefore, they are not suitable for healthcare applications, especially at lower sampling rates. For the WT filter bank, F23 performs better than the other two filters in both phases in terms of absolute error.

At the same time, the anomaly of F21 in absolute error at 1000 Hz can be seen in the table. This could be due to the unsuitable selection of the mother wavelets.

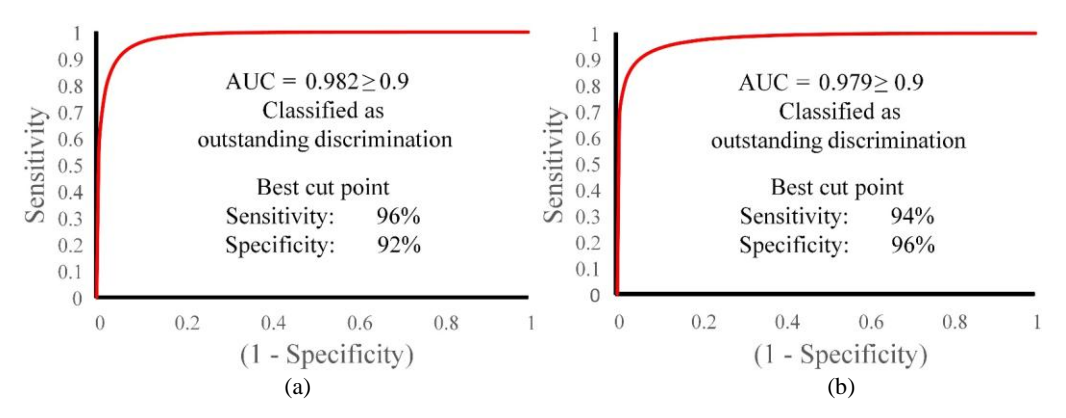


Fig. 7. Evaluation of the best SSIV assessment range of normal cardiac autonomic function with the ROC curve, (a) – the resting phase; (b) – the deep breathing phase.

B. Evaluation of interbeat variation and HRV in PPGs

In Table 2, three parameters related to heart rhythm variability, SSIV, SDNN, and NN50, were used to evaluate the accuracy of using PPG instead of ECG. Since the calculation of the absolute errors of these parameters is performed using (4), the units of measurement for the absolute errors are expressed in percent (%) for SSIV and NN50 and in ms for SDNN.

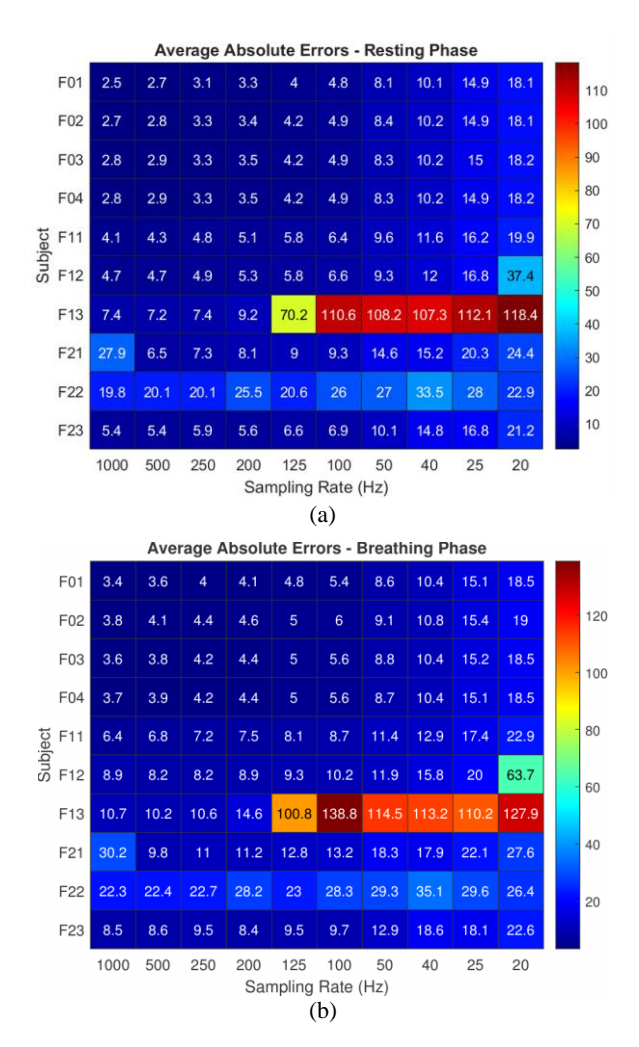


Fig. 8. HeatMap of average absolute errors between the RRI at 1000 Hz and the SSIs at different sampling rates in resting (a) and breathing phases (b).

The evaluation tests showed the average absolute errors of SSIV, SDNN, and NN50 from the filters F01, F11, and F23 at different sampling rates, related to the test phase in Table 2. The F01 IIR filter bank produces the most accurate values for SSIV, SDNN, and NN50 compared to all other filters, and F01 in particular achieves the best accuracy. In addition, F11 and F23 showed very low average absolute errors in their respective filter bank, as can be seen in Fig. 8.

In addition, F23 shows greater superiority than F11 as the accuracy values are better at the lower sampling rates of Table 2. This indicates that the WT filters have good potential for use in wearable healthcare applications.

C. ANS screening for healthcare application

Table 3 shows the RRIV assessment range for normal cardiac autonomic function during the resting and deep breathing phases of an outpatient neurological examination [31]. Due to the superiority of acquiring PPG signals over ECG, the idea of replacing the ECG data in Table 3 with the PPG data based on the previous analysis is very promising for remote healthcare monitoring.

To obtain a case of the most appropriate SSIV assessment range for normal cardiac autonomic function, it is necessary to find the best SSIV assessment range based on a set of optimal sensitivity and specificity values of the statistical test results. To give an example, the SSIV result with a 1000 Hz sampling rate from the Butterworth filter (F01) was used with the previous correlation and accuracy analysis.

To replace RRIV with SSIV in Table 3, the RRIV and SSIV values of all participants, totaling 244 cases, were screened and confirmed by the neurologist in our research team to determine whether their cardiac ANS was normal or abnormal. Subsequently, the diagnostic results are treated with RRIV as the ground truth and the SSIV results are the predictive values. Table 4 shows a confusion matrix based on the RRIV ground truth and SSIV substitution value, with the SSIV assessment range values for all age groups taken from Table 3. In this case, the calculated sensitivity and specificity, which are 86.27 % and 98.45 % for the resting phase and 84.62 % and 98.96 % for the deep breathing phase, are shown in the column 'RRIV source' in Table 5.

To obtain the most appropriate normal assessment range of the SSIV, an inward/outward scaling strategy using the ROC curve is attempted [37]. For a scale-out increment of 1, the scope of the RRIV assessment range (Table 3) is extended by decreasing the lower limit of the range by 1 and increasing the upper limit of the range by 1. For example, the normal assessment range in the resting phase for the 20 to 29 year olds is $12 \sim 46$ ms; if the normal assessment range is in a scale-out increment of 2, it becomes $10 \sim 48$ ms; and if the range is decreased inward by 4, it becomes $16 \sim 42$ ms. Apply the same inward/outward scaling strategy for other age groups. In Table 5, the term 'Out+2' means that the normal assessment range is in a scale-out increment of 2, and 'In-4' means that the range decreases inward by 4. Consequently, Table 5 shows seven possible prediction models with sensitivity and specificity for different increments and decrements. Note that the term 'RRIV source' denotes an increment or decrement of 0.

Table 4. Confusion matrix between RRIV and SSIV in the resting and deep breathing phases.

		RRIV	RRIV
Phase	SSIV	Abnormal	Normal
		[ms]	[ms]
Docting	Abnormal	44	2
Resting	Normal	8	190
Doon broothing	Abnormal	44	3
Deep breathing	Normal	7	190

As a screening tool for daily life, the best normal assessment range of the SSIV should have the characteristic of high sensitivity and low (1 - specificity), resulting in most true positives being positive and few true negatives being positive. Based on the seven SSIV prediction models in Table 5, the ROC curves of the resting and deep breathing phases are outlined in Fig. 5. In Fig. 7, the sensitivity and specificity of the best cut-off point are 96 % and 92 % in the resting phase, and 94 % and 96 % in the deep breathing phase, respectively. It can be seen that the SSIV assessment range of 'In-1' in Table 5 comes closest to the best cut points for both phases.

In addition, Fig. 7 shows an evaluation index, namely the area under the curve (AUC). In the ROC curves, the AUC indicates the discrimination capacity of an SSIV prediction model. In the case of Fig. 7, the AUC of the resting and deep breathing phases are 0.982 and 0.979, respectively. If the value of the AUC is greater than 0.9, the SSIV prediction model has excellent discrimination. As a screening tool, this result is very accurate and sufficient. The most appropriate SSIV assessment range is shown in Table 6.

Table 5. The sensitivity and specificity of SSIV in different assessment ranges.

Phase	Rate [%]	Out+2	Out+1	RRIV source	In-1	In-2	In-3	In-4
Rest	Sensitivity	36.54	63.46	84.62	96.15	96.15	100.00	100.00
	Specificity	98.96	98.96	98.96	91.67	79.69	70.83	59.90
Decath	Sensitivity	54.90	70.59	86.27	94.12	94.12	96.08	96.08
Breath	Specificity	99.48	99.48	98.45	95.85	91.19	84.97	78.24

Table 6. SSIV assessment range of normal cardiac autonomic function in each age group based on PPG.

Age [y]	20 ~ 29	30 ~ 39	40 ~ 49	50 ~ 59	60 ~ 69
Rest [ms]	13 ~ 45	7 ~ 31	7 ~ 35	6 ~ 22	8 ~ 18
Breath [ms]	20 ~ 61	10 ~ 53	15 ~ 47	12 ~ 58	9 ~ 27

5. DISCUSSION

The evaluation of accuracy and correlation shows the close relationship between RRI at 1000 Hz and SSI at different sampling rates. Table 2 and Table 3 confirm that the IIR filter bank performs very well even at 40 Hz in the two test phases, and F11 and F23 have similar results. When evaluating the variability of the heart rhythm with PPG, the IIR filter bank showed the best accuracy, regardless of the test phase. F12 produced the worst SSIVs in both phases in the FIR and WT filter banks. One possible reason for this is that the detection results of the peak detection scheme deviate significantly from the true peak position. Moreover, F12 and F13 are not both of poor accuracy. Their poor accuracy only occurs at frequencies below 200 Hz and 25 Hz, respectively. Therefore, their availability still depends on application requirements.

As for the FIR filter bank, its performance is not as good as that of the IIR filters. These filters are better at smoothing

and filtering out noise outside the signal band, but when noise is embedded in the signal band, the detected signal peaks used to determine the SSIs deviate accordingly, making the absolute error higher. However, it seems that only F11 can better deal with the problem of signal peak deviation due to embedded noise in the signal. For the filter bank of the wavelet transform, it can be seen that F23 outperforms the other two DWT methods. This is due to the fact that their mother wavelets are not close to the morphology of the PPG signal curves. In contrast, the mother wavelet of F23 is more closely related to the PPG morphology, so its accuracy and correlation are better than those of the other two methods.

For the normal assessment range of cardiac autonomic function suitable for SSIV, the discriminating capacity of the assessment in the two phases is 0.982 and 0.979, respectively, which is recognized as excellent. In practice, it shows that it is possible to detect autonomic abnormalities by calculating and extracting SSIV values from the processed PPG signals at different sampling rates.

6. CONCLUSION

Compared to previous studies, our approach stands out in that we systematically evaluate multiple filter types across a range of sampling rates, which is rarely addressed in the current literature. Most existing work relies on a fixed filter or sampling configuration, often optimized for controlled environments or non-clinical applications [4], [5], [21]. Although some studies show acceptable accuracy for general HR estimation, they are not robust enough when applied to clinical use cases such as the detection of cardiac autonomic neuropathy. In contrast, our study provides a comprehensive performance comparison showing that filters such as Butterworth and Morlet wavelets exhibit high fidelity in peak detection and HRV feature extraction even at low sampling rates and variable conditions. This fills a significant research gap and lays the foundation for more reliable PPG-based diagnostics in both clinical and wearable settings.

In the literature, some studies focus on heartbeat and heart rate detection with wearable devices in daily life, which cannot provide sufficiently accurate PPG features. It is clear that anti-noise filters performed with different sampling rates have not been extensively evaluated, especially for clinical trials using SSIV to detect cardiac autonomic neuropathy. In this study, PPG was investigated as an alternative to ECG to detect cardiac autonomic neuropathy. Since PPG is susceptible to noise due to motion artifacts, suitable filters for different sampling rates need to be tested for noise immunity.

All PPG signals were processed and screened for the target application of detecting autonomic abnormalities. In the experiments, we found that the Butterworth, Bessel, Chebyshev, Elliptic, and Savitzky-Golay filters and the Morlet wavelet have the best signal preprocessing capabilities for the 10 selected sampling rates and thus can accurately localize the peaks in the PPG signal to generate interbeat intervals. We also investigated these filters to generate other PPG-derived parameters such as the interbeat variation, SDNN, and NN50. The results show that the above filters are still good candidates for the intended application. Finally, the normal range of autonomic nerves suitable for SSIV was determined by ROC curve analysis. The AUC in the resting phase was as high as 98.2 % and in the deep breathing phase reached 97.9 %. In conclusion, the IIR filter bank, F11 and F23 can provide very satisfactory processing results for wearable healthcare applications with lower acquisition rates.

In addition to healthcare monitoring and clinical screening, PPG applications in disease-related screening require highly accurate signal processing. For example, participants with severe peripheral artery atherosclerosis, including subclavian or brachial artery stenosis, may affect the systolic peak of pulsation, and the PPG signal is easily disturbed by hand movements, an uncooperative participant or those with obvious tremor or dyskinesia may not record reliable results. In this study, we have only completed the exploration of interbeat variation and HRV time-domain parameters. In the near future, we need to investigate other parameters suitable for disease detection. To explore PPG-based blood pressure blood glucose estimation, biometric identification, etc. in depth, a lot of research work needs to be done in the future.

ACKNOWLEDGMENT

This work was financially supported by the National Taiwan University Hospital Yunlin Branch under the medical research project [NTUHYL108.C010]. Additional support was provided by the "Intelligent Recognition Industry Service Center" of the Featured Areas Research Center-Program, within the framework of the Higher Education Sprout Project by the Ministry of Education (MOE) in Taiwan. The authors also gratefully acknowledge partial funding from the Ministry of Science and Technology, Taiwan [MOST 108-2637-E-224-002, MOST109-2637-E-224-001]. The sponsors played no role in the study design, data collection and analysis, data interpretation, and manuscript preparation. We especially thank Zheng-Wei Lai and Ying-I Tang for their excellent contributions to the signal processing tasks.

REFERENCES

- [1] Shahani, B. T., Day, T. J., Cros, D., Khalil, N., Kneebone, C. S. (1990). RR interval variation and the sympathetic skin response in the assessment of autonomic function in peripheral neuropathy. *Archives of Neurology*, 47 (6), 659-664. https://doi.org/10.1001/archneur.1990.0053006006902
- [2] Stålberg, E. V., Nogués, M. A. (1989). Automatic analysis of heart rate variation: I. Method and reference values in healthy controls. *Muscle & Nerve*, 12 (12), 993-1000. https://doi.org/10.1002/mus.880121207
- [3] Kano, Y., Yoshizawa, M., Sugita, N., Abe, M., Homma, N., Tanaka, A., Yamauchi, T., Miura, H., Shiraishi, Y., Yambe, T. (2014). Discrimination ability and reproducibility of a new index reflecting autonomic nervous function based on pulsatile amplitude of photoplethysmography. In 2014 36th Annual International Conference of the IEEE Engineering in Medicine and Biology Society. IEEE, 1794-1800. https://doi.org/10.1109/EMBC.2014.6943957
- [4] Moreno, S., Quintero-Parra, A., Ochoa-Pertuz, C., Villarreal, R., Kuzmar, I. (2018). A signal processing method for respiratory rate estimation through photoplethysmography. *International Journal of Signal Processing, Image Processing and Pattern Recognition*, 11 (2), 1-10. http://dx.doi.org/10.14257/ijsip.2018.11.2.01
- [5] Chang, Y.-W., Hsiu, H., Yang, S.-H., Fang, W.-H., Tsai, H.-C. (2016). Characteristics of beat-to-beat photoplethysmography waveform indexes in subjects with metabolic syndrome. *Microvascular Research*, 106, 80-87. https://doi.org/10.1016/j.mvr.2016.04.001
- [6] Du, Y.-C., Stephanus, A. (2018). The feasibility study of photoplethysmography features for arteriovenous fistula stenosis detection in hemodialysis patients with statistical approach. In 2018 IEEE International Conference on Applied System Invention (ICASI). IEEE, 457-460.

https://doi.org/10.1109/ICASI.2018.8394284

[7] Smith, R. P., Argod, J., Pépin, J.-L., Lévy, P. A. (1999). Pulse transit time: An appraisal of potential clinical applications. *Thorax*, 54 (5), 452-457. https://thorax.bmj.com/content/54/5/452

- Friesen, G. M., Jannett, T. C., Jadallah, M. A., Yates, S. [8] L., Quint, S. R., Nagle, H. T. (1990). A comparison of the noise sensitivity of nine QRS detection algorithms. IEEE Transactions on Biomedical Engineering, 37 (1), 85-98. https://doi.org/10.1109/10.43620
- Middleton, P. M., Chan, G. S., O'Lone, E., Steel, E., Carroll, R., Celler, B. G., Lovell, N. H. (2009). Changes in left ventricular ejection time and pulse transit time derived from finger photoplethysmogram electrocardiogram during moderate haemorrhage. Clinical Physiology and Functional Imaging, 29 (3), 163-169.
 - https://doi.org/10.1111/j.1475-097X.2008.00843.x
- [10] Shouran, M., Elgamli, E. (2020). Design and implementation of Butterworth filter. International Journal of Innovative Research in Science, Engineering and Technology, 9 (9), 7975-7983.
- [11] Bowman, F. (2012). Introduction to Bessel Functions. Courier Corporation, ISBN 9780486152998.
- [12] Lutovac, M. D., Tošić, D. V., Evans, B. L. (2000). Filter Design for Signal Processing using MATLAB and Mathematica. Prentice Hall, ISBN 9780201361308.
- [13] Lin, L., Liu, T., Yuan, N., Xu, Z., Chen, H. (2021). Study on the influence of venturi on the cleaning performance of elliptical filter cartridge. Powder Technology, 377, 139-148. https://doi.org/10.1016/j.powtec.2020.08.097
- [14] Abinaya, M., Prabhakaran, S., Jaisankar, N. (2014). Photoplethysmography on smart phone using Savitzky-Golay filter. International Journal of Scientific & Engineering Research, 5 (6).
- [15] Gonzalez, R. C., Woods, R. E. (2007). Digital Image Processing. Pearson, ISBN 978-0131687288.
- [16] Lee, H.-W., Lee, J.-W., Jung, W.-G., Lee, G.-K. (2007). The periodic moving average filter for removing motion artifacts from PPG signals. International Journal of Control, Automation, and Systems, 5 (6), 701-706.
- [17] Sahoo, A., Manimegalai, P., Thanushkodi, K. (2011). Wavelet based pulse rate and Blood pressure estimation system from ECG and PPG signals. In 2011 Conference Computer, International onCommunication and Electrical Technology (ICCCET). IEEE, 285-289. https://doi.org/10.1109/ICCCET.2011.5762486
- [18] Lee, H.-K., Heo, I., Yang, S., Lee, K.-J. (2014). Discrete wavelet transform-based method for automatic evaluation of sleep-disordered breathing using photoplethysmography. In 2014 5th International Conference on Intelligent Systems, Modelling and Simulation. IEEE, 206-208. https://doi.org/10.1109/ISMS.2014.41
- [19] Wu, B.-F., Huang, P.-W., Tsou, T.-Y., Lin, T.-M., Chung, M.-L. (2017). Camera-based Heart Rate measurement using continuous wavelet transform. In 2017 International Conference on System Science and Engineering (ICSSE). IEEE, 7-11. https://doi.org/10.1109/ICSSE.2017.8030826

- [20] Zhong, Y., Pan, Y., Zhang, L., Cheng, K.-T. (2016). A wearable signal acquisition system for physiological signs including throat PPG. In 2016 38th Annual International Conference of the IEEE Engineering in Medicine and Biology Society (EMBC). IEEE, 603-606. https://doi.org/10.1109/EMBC.2016.7590774
- [21] Pietilä, J., Mehrang, S., Tolonen, J., Helander, E., Jimison, H., Pavel, M., Korhonen, I. (2018). Evaluation accuracy and reliability photoplethysmography based heart rate and beat-tobeat detection during daily activities. In IFMBE Proceedings, 65, 145-148.
 - https://doi.org/10.1007/978-981-10-5122-7_37
- [22] Chatterjee, A., Prinz, A. (2018). Image analysis on fingertip video to obtain PPG. Biomedical and Pharmacology Journal, 11 (4), 1811-1827. https://dx.doi.org/10.13005/bpj/1554
- [23] Hosni, A., Atef, M. (2023). Remote real-time heart rate monitoring with recursive motion artifact removal using PPG signals from a smartphone camera. Multimedia Tools and Applications, 82 (13), 20571-20588. https://doi.org/10.1007/s11042-023-14399-w
- [24] Ebrahimi, Z., Gosselin, B. (2023). Ultralow-power photoplethysmography (PPG) sensors: methodological review. IEEE Sensors Journal, 23 (15), 16467-16480. https://doi.org/10.1109/JSEN.2023.3284818
- [25] Chu, Y., Tang, K., Hsu, Y.-C., Huang, T., Wang, D., Li, W., Savitz, S. I., Jiang, X., Shams, S. (2023). Noninvasive arterial blood pressure measurement and SpO2 estimation using PPG signal: A deep learning framework. BMC Medical Informatics and Decision Making, 23 (1), 131. https://doi.org/10.1186/s12911-023-02215-2
- [26] Liu, X., Narayanswamy, G., Paruchuri, A., Zhang, X., Tang, J., Zhang, Y., Sengupta, R., Patel, S., Wang, Y., McDuff, D. (2023). rPPG-toolbox: Deep remote PPG toolbox. In Proceedings of the 37th International Conference on Neural Information Processing Systems. New York, US: Curran Associates Inc., 68485-68510.
- [27] Baltrusaitis, T., Zadeh, A., Lim, Y. C., Morency, L.-P. (2018). OpenFace 2.0: Facial behavior analysis toolkit. In 2018 13th IEEE International Conference on Automatic Face & Gesture Recognition. IEEE. https://doi.org/10.1109/FG.2018.00019
- [28] Huang, B., Chen, W., Lin, C.-L., Juang, C.-F., Wang, J. (2022). MLP-BP: A novel framework for cuffless blood pressure measurement with PPG and ECG signals based on MLP-Mixer neural networks. Biomedical Signal Processing and Control, 73, 103404. https://doi.org/10.1016/j.bspc.2021.103404
- [29] Peláez-Coca, M. D., Hernando, A., Lázaro, J., Gil, E. (2022). Impact of the PPG sampling rate in the pulse rate variability indices evaluating several fiducial points in different pulse waveforms. IEEE Journal of Biomedical and Health Informatics, 26 (2), 539-549. https://doi.org/10.1109/JBHI.2021.3099208

- [30] Burma, J. S., Griffiths, J. K., Lapointe, A. P., Oni, I. K., Soroush, A., Carere, J., Smirl, J. D., Dunn, J. F. (2024). Heart rate variability and pulse rate variability: Do anatomical location and sampling rate matter? *Sensors*, 24 (7), 2048. https://doi.org/10.3390/s24072048
- [31] ADInstruments. *Labchart 5 software adinstruments owners manual*. https://www.adinstruments.com/products/labchart
- [32] de Chazal, P., Heneghan, C., Sheridan, E., Reilly, R., Nolan, P., O'Malley, M. (2003). Automated processing of the single-lead electrocardiogram for the detection of obstructive sleep apnoea. *IEEE Transactions on Biomedical Engineering*, 50 (6), 686-696. https://doi.org/10.1109/TBME.2003.812203
- [33] Liu, S., Ni, H., Zhong, Y., Yan, W., Wang, W. (2025). Adaptive weighted median filtering for time-varying graph signals. *Signal, Image and Video Processing*, 19 (1), 88. https://doi.org/10.1007/s11760-024-03610-6
- [34] Pan, J., Tompkins, W. J. (1985). A real-time QRS detection algorithm. *IEEE Transactions on Biomedical Engineering*, 32 (3), 230-236. https://doi.org/10.1109/TBME.1985.325532
- [35] Saritha, C., Sukanya, V., Narasimha Murthy, N. (2008). ECG signal analysis using wavelet transforms. *Bulgarian Journal of Physics*, 35 (1), 68-77.
- [36] Task Force of the European Society of Cardiology the North American Society of Pacing Electrophysiology. (1996). Heart rate variability: Standards of measurement, physiological interpretation, and clinical use. *Circulation*, 93 (5), 1043-1065. https://doi.org/10.1161/01.CIR.93.5.1043

- [37] Florkowski, C. M. (2008). Sensitivity, specificity, receiver-operating characteristic (ROC) curves and likelihood ratios: Communicating the performance of diagnostic tests. *Clinical Biochemist Reviews*, 29 (Suppl 1), S83-S87.
- [38] Chiang, M.-C., Yeh, T.-Y., Sung, J.-Y., Hsueh, H.-W., Kao, Y.-H., Hsueh, S.-J., Chang, K.-C., Feng, F.-P., Lin, Y.-H., Chao, C.-C., Hsieh, S.-T. (2021). Early changes of nerve integrity in preclinical carriers of hereditary transthyretin Ala117Ser amyloidosis with polyneuropathy. *European Journal of Neurology*, 28 (3), 982-991. https://doi.org/10.1111/ene.14698
- [39] ADInstruments. (2014). *PowerLab teaching series: Owner's guide*. Document no. U-ML818/OG-003F.
- [40] Umar, L., Firmansyah, I., Setiadi, R. N. (2018). Design of pulse oximetry based on photoplethysmography and beat rate signal using DS-100 probe sensor for SpO 2 measurement. In 2018 3rd International Seminar on Sensors, Instrumentation, Measurement and Metrology (ISSIMM). IEEE, 25-29. https://doi.org/10.1109/ISSIMM.2018.8727725
- [41] Sáringer, S., Kaposvári, P., Benyhe, A. (2024). Visual linguistic statistical learning is traceable through neural entrainment. *Psychophysiology*, 61 (8), e14575. https://doi.org/10.1111/psyp.14575

Received October 8, 2024 Accepted July 2, 2025